ELSEVIER

Journal of Nuclear Materials 266–269 (1999) 507–512

journal of nuclear materials

Radiation measurements and modeling of the density limit on the W7-AS stellarator

L. Giannone *, R. Burhenn, P. Grigull, U. Stroth, R. Brakel, R. Dux, A. Elsner, S. Fiedler, G. Kühner, F. Penningsfeld, G. Pereverzev, F. Wagner, A. Weller, C. Wendland, NBI Team, W7-AS Team

Max-Planck-Institut für Plasmaphysik, EURATOM Association, D-85748 Garching, Germany

Abstract

Density limit discharges in the W7-AS stellarator with a strong density ramp were compared to a series of discharges with constant line integrated density approaching the maximum value achieved in the density ramp. The physics of the density limit in stellarators was demonstrated to be consistent with the predictions of the two-point model, indicating that this model successfully describes the density limit process in both stellarators and tokamaks. The discharges with a strong density ramp were found to have broader density profiles than those discharges with constant line integrated density. The latter discharges had the electron density profile form found in the improved confinement H-NBI mode on W7-AS. Modeling of the radiation profile, to simultaneously match the measured bolometer and soft X-ray radial profiles of radiated power, implies that impurity density profiles were peaked and continuously increased during the discharge. The increase in radiated power decreased the net deposited power to the plasma and the diamagnetic energy fell. The aim of producing steady-state discharges at the highest possible density is aided by the reduction of impurity sources by helium glow discharge cleaning.

Keywords: Density limit; Modeling; W7-AS

1. Introduction

In W7-AS, a discharge with rising line integrated electron density reaches a maximum density, then the diamagnetic energy falls and the radiated power rises continuously until the discharge terminates. This maximum density defines the density limit in W7-AS. Discharges with a constant line integrated density (density plateau) were also studied. In discharges at successively higher density plateaus, the rate of diamagnetic energy decrease after the peak in diamagnetic energy was larger at higher densities. Decreasing net power to the plasma due to core radiation is believed to be responsible for the observed fall in diamagnetic energy.

The density profiles in discharges with a density ramp were markedly broader than those with a density plateau. These density plateau discharges are therefore closely related to the improved confinement scenario in W7-AS (H-NBI mode) but at densities in the vicinity of the density limit [1]. At sufficiently low densities, discharges of duration up to 1.8 s were possible. Such experiments in both tokamaks and stellarators are relevant to the future operation scenario of a reactor, as sustainable steady state high-density discharges will be required for power handling and ignition [2].

Measurements of the time evolution of the density and temperature in front of the limiter were compared with predictions of simulations by the time dependent transport code ASTRA [3] combined with a one-dimensional scrape-off layer model of the plasma edge (the two-point model) [4]. The addition of the impurity transport code STRAHL [5] allowed radiation profile measurements of the bolometer and soft X-ray cameras to be simulated. The increase in radiated power during density plateau discharges was due to a central peaking

* Corresponding author. E-mail: giannone@ipp.mpg.de.

0022-3115/99/$ – see front matter
PII: S0022-3115(98)00671-0

of the radiation power density. Such a peaking has been observed previously in the W-VIIA stellarator [6] and accounted for by neoclassical impurity transport of oxygen ions from the vessel walls and tungsten from the NI beams. In W7-AS, 3% shine through losses and 2% charge-exchange losses were calculated. Impurity ions, produced by energetic ions impinging on the wall, could therefore have been a relevant factor in the observed discharge evolution.

2. Two-point model

Simulations of the time evolution of the electron density and temperature measurements in front of the limiter were carried out with the time dependent transport code ASTRA. This code solves the particle balance, electron energy power balance and ion energy power balance equations as a function of time, allowing time dependent simulations to be carried out. The equations are one-dimensional and averaged over closed magnetic flux surfaces. A module was added to ASTRA to describe the physics of the scrape-off layer in terms of the two-point model. The two-point model is a one-dimensional model based on electron heat conduction and pressure balance along the field line from the last closed flux surface to a limiter or divertor plate [4] and the predictions of this model have been shown to be consistent with observations in density limit experiments in limiter discharges in a tokamak [7]. A modified pressure balance equation along field lines to account for momentum loss effects due to ion-neutral friction is used [8]:

$$T_{\mathrm{es}} = \left(T_{\mathrm{ed}}^{7/2} + \frac{7}{4\kappa_0} q_{//\mathrm{s}} L_{\mathrm{c}} \right)^{2/7} \left(1 - \left(\frac{T_{\mathrm{ed}}}{T_{\mathrm{es}}} \right)^{7/2} \right)^{-2/7}. \quad (1)$$

$$2 n_{\mathrm{ed}} T_{\mathrm{ed}} = f_m n_{\mathrm{es}} T_{\mathrm{es}}, \quad (2)$$

where n_{es} and T_{es} are the density and temperature at the last closed flux surface, n_{ed} and T_{ed} are the density and temperature in front of the limiter, L_{c} is the connection length from the last closed flux surface to the limiter (typically 30–100 m depending on the poloidal angle), κ_0 is the factor in the electron thermal conductivity equation, f_m is the reduction factor in pressure along the field line and Δ_T is the temperature fall off length in the scrape-off layer. The parallel heat flux to the limiter, $q_{//\mathrm{s}}$, given by the perpendicular heat flux at the last closed flux surface, $q_\perp$, multiplied by the geometrical factor, L_{c}/Δ_E. The heat flux across a flux tube of length L_{c} is projected onto the limiter within an energy fall length $\Delta_E = 2/7\ \Delta_T$. This parallel flux to the limiter is balanced by the sum of losses by ionization of neutrals, by impurity radiation and in the sheath in front of the limiter or divertor plate

$$q_{//\mathrm{s}} = 7 L_{\mathrm{c}} q_\perp / 2\Delta_T = n_{\mathrm{D}} c_{\mathrm{S}} \beta\xi + c_{\mathrm{rad}} l \gamma_{\mathrm{imp}} n_{\mathrm{D}}^2 + \gamma n_{\mathrm{D}} T_{\mathrm{D}} c_{\mathrm{S}}. \quad (3)$$

These equations can be solved for n_{ed}, T_{ed} and T_{es}, using n_{es} and $q_\perp$ as inputs.

3. Density ramps

The lithium beam diagnostic measures the time evolution of the radial profile of n_{e}, therefore providing the input value of n_{es}. The total radiated power is deduced from Abel inverted measurements of the line integrated power flux onto 4 μm gold foil absorbers of a 12 channel bolometer array and then $q_\perp$ is calculated from the deposited neutral beam injection (NBI) power minus the total radiated power. The soft X-ray measurements are carried out with two cameras, each of 36 channels, of surface barrier diodes. The placement of a 12.5 μm beryllium foil in front of the entrance slit allows the filtering out of energy components below 1 keV.

A discharge at $B = 2.5$ T with 380 kW of NBI heating and a density ramp that increased the central density from 5.5×10^{19} to 1.5×10^{20} m^{-3} in the time interval from 0.2 to 0.6 s is shown in Fig. 1. The magnetic configuration, with an edge value of rotational transform, ι of 0.34 is bounded by two tangential graphite limiters at the top and bottom of an elliptical cross-section of magnetic flux surfaces. A comparison of the Langmuir probe measurements of n_{ed} and T_{ed} and the predictions of the modified two-point model are also shown. The evolution of n_{ed} and T_{ed} are reasonably simulated with a continuously falling temperature and a density reaching a maximum at 0.5 s and a continuously falling temperature. In agreement with the usual description of the density limit in tokamaks, a critical edge density is reached at which the value of net power flux can no longer sustain power balance in front of the limiter and detachment from the limiter follows [9]. The physics of the density limit in stellarators can therefore be adequately described by the two-point model indicating that this model describes the density limit process in both stellarators and tokamaks. After 0.56 s the radiated power is greater than the deposited power and the discharge rapidly collapses. However, no tearing mode instability is triggered in a stellarator in contrast to observations of the density limit on a tokamak [10]. The difference in maximum value of density in front of the limiter predicted and observed, may be partially explained by the overestimation of the measured electron temperature suggested to occur in the presence of non-thermal electrons from the upstream plasma [9]. From the Langmuir probe measurements of ion saturation current, the calculated density is then underestimated.

Discharges with a Murakami parameter greater than the Greenwald limit were achieved transiently in W7-AS in this set of discharges. Similarly plasma parameters

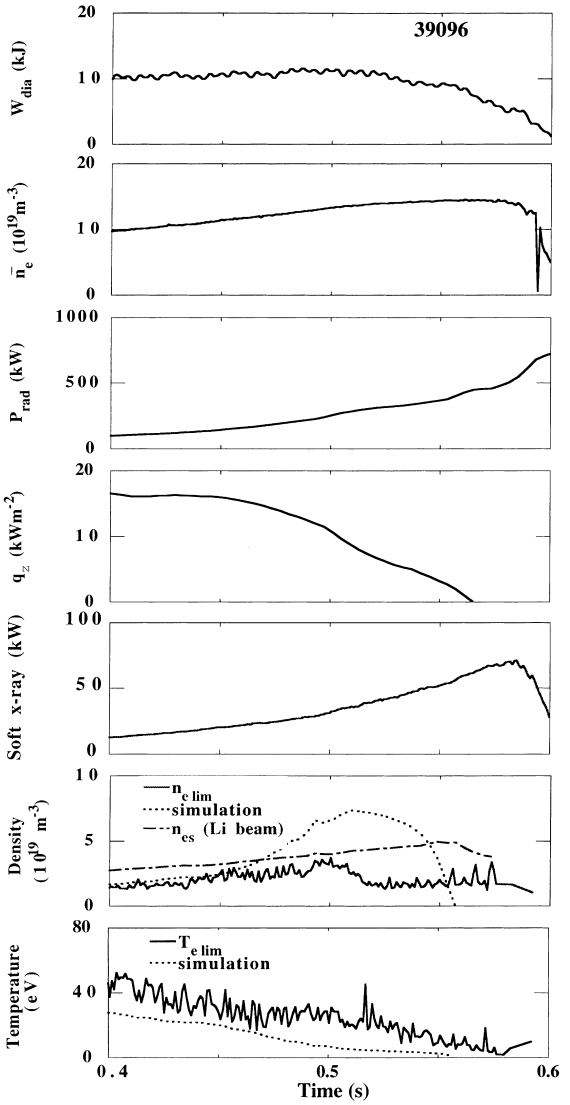

Fig. 1. Diamagnetic energy, line integrated density, radiated power and net heat flux at the plasma edge for a density limit discharge with a density maximum in front of the limiter at 0.5 s followed by detachment and a fall in the diamagnetic energy. After 0.56 s the radiated power is greater than the deposited power and the plasma collapses rapidly. The time evolution of the density and temperature in front of the limiter is compared to the calculated values from the modified two-point model.

yielding values above the Greenwald limit in tokamak density limit discharges have also been achieved transiently using pellet injection [11] or for a duration of 0.8 s with only a slow increase of radiated power [12]. Such global comparisons will be extended in the near future by measurements at the density limit of local electron density and temperature inside the last closed flux surface to compare to the edge operational diagram for tokamaks [13]. A sequence of energy detachment, an edge thermal instability, particle detachment and disruption at the density limit is observed below a critical edge temperature and above a critical edge density [14].

4. Density plateaus

Discharges at $B = 2.5$ T with 380 kW of NBI heating at successively higher line averaged densities starting from 5.5×10^{19} to 8.0×10^{19} m^{-2} or peak densities of 1.1–1.6×10^{20} m^{-3} showed that for each density plateau a peak in the diamagnetic energy was reached and that the level of radiated power rose during the discharge. Again the magnetic configuration was bounded by the two tangential limiters at the top and bottom of an elliptical cross-section for discharges with $\frac{1}{\epsilon}$ of 0.34. The limiter radius was at $r = 16.2$ cm. The diamagnetic energy decreased faster in those discharges at higher density. In Fig. 2, density plateau discharges before and after helium glow discharge cleaning at a density of 1.3×10^{20} m^{-3} display the extent to which wall conditioning can influence the time evolution. At a lower density the discharge takes longer to collapse because the radiated power does not increase to the same level so quickly. A simple explanation is that the impurity particle flux is drastically reduced. The particle flux to the limiter, as measured by the ion saturation current to a Langmuir probe embedded there, did not change after helium glow discharge cleaning. This indicates that the source of impurity ions at the surface have been modified by the discharge cleaning.

In addition to possible changes in the impurity flux, density and temperature profile changes or a change in particle or heat transport coefficients are also factors determining the evolution of the radiation profiles. At present, only the time evolution of the central electron temperature from Thomson scattering was available and the temperature profile from a single time point was scaled appropriately. Under these experimental limitations a detailed analysis is not possible. This analysis can be performed when the profiles of density and temperature from Thomson scattering every 50 ms are available in the near future. It will be then also possible to calculate the change in impurity flux at the boundary needed to adequately simulate the discharge prior to discharge cleaning.

The density profile evolution was measured by the lithium beam diagnostic. Even though the level of gas puffing is reduced after 0.5 s, the central density slowly increased and the density at $r = 10$ cm remained approximately constant, indicating a peaking of the density profile during the discharge. The increasing central electron density and consequent plasma cooling is one factor involved in the observed deterioration in diamagnetic energy during the discharge.

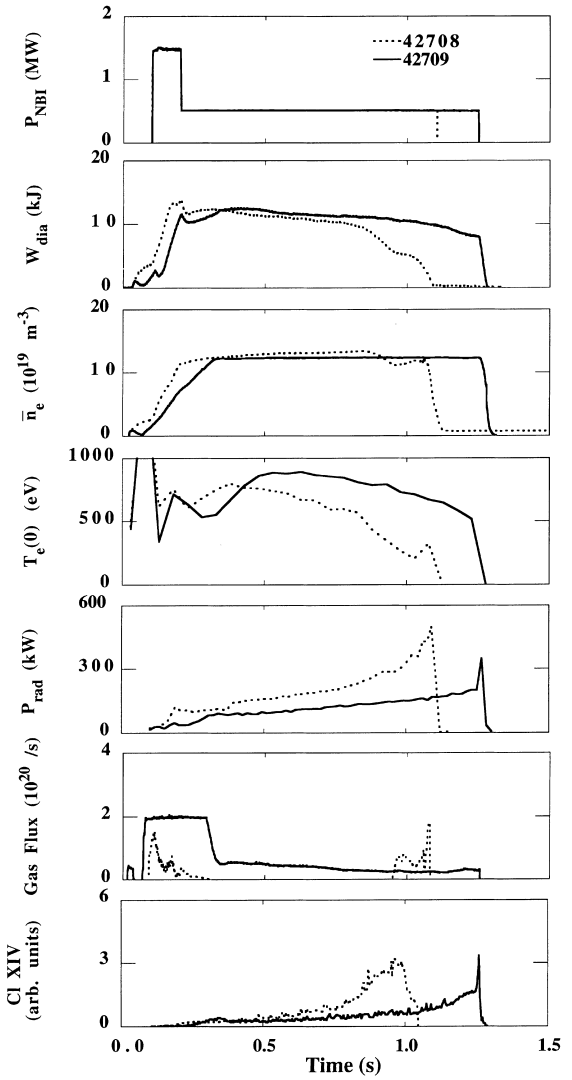

Fig. 2. Comparison of a density plateau discharge near the density limit before and after glow discharge cleaning. After the peak in diamagnetic energy is reached a slow decay is observed concurrent with increasing radiated power. After glow discharge cleaning the impurity flux to the plasma is significantly reduced and a marked reduction in radiated power is the result. The electron density profile slowly rises but the profile becomes narrower while the central electron temperature decreases with time.

5. Radiation profiles

The radial profiles of the diffusion coefficient, D and inward pinch velocity, v, shown in Fig. 3 were calculated from measurements of the time evolution soft X-ray emission and Al impurity lines after aluminum impurity injection by laser blow-off [15]. The Al impurity lines were measured by a Jobin–Yvon spectrometer (Al XI)

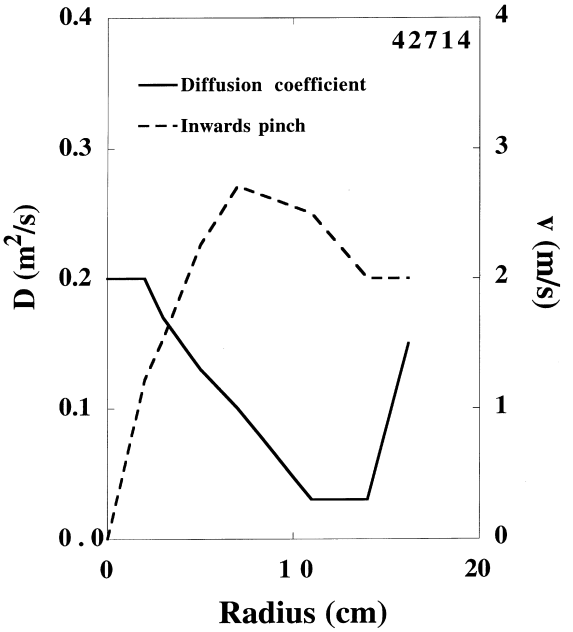

Fig. 3. Following aluminum impurity injection by laser blow-off, the time evolution soft X-ray measurements with a 25 μm Be filter and Al impurity lines (XI, XII) are used to derive radial profiles for the diffusion coefficient, D and inward pinch velocity, v.

and a Bragg spectrometer (Al XII). The soft X-ray emission with and without impurity injection are subtracted to yield the net emission due to impurity injection. The electron density profiles of this discharge were within 10% of the density plateau discharge after helium glow discharge cleaning shown in Fig. 2. It should be noted that the following simulation of this density plateau discharge assumes that the measured diffusion coefficient and inward pinch velocity do not change significantly with density or density profile during the discharge.

Spectroscopic measurements of line radiation by the SPRED VUV spectrometer showed that the impurity elements carbon, chlorine and copper were dominant in the density limit discharges studied. Using the radial profiles of D and v derived from laser blow-off experiments, together with the time evolution of the density and temperature profiles and an assumed constant impurity flux of each impurity at the boundary, simulations of the time evolution of bolometer and soft X-ray radiation profiles were carried out with the impurity transport code, STRAHL. This code calculates the impurity ion balance of a single impurity species according to the input parameters described and uses tabulated atomic rate coefficient data for ionization, radiative recombination, dielectronic recombination and charge-exchange recombination to calculate the radiated power

as a function of minor radius in the plasma. In Fig. 4, the measured and simulated radiation profiles for the bolometer and soft X-ray (12.5 μm beryllium foil filter) cameras for the density plateau discharge considered in Fig. 2 are compared. These simplified assumptions are sufficient to satisfactorily simulate the peaking of the measured bolometer and soft X-ray profiles. Maximum central relative impurity densities at the end of the discharge for carbon, chlorine and copper of 0.057, 0.004 and 0.0005 respectively and therefore a Z_{eff} of 3.6, were estimated. The contribution to the radiated power density for the bolometer measurements in the center is in roughly equal proportions for each impurity element, while for the soft X-ray measurements they were 16%, 50% and 34%, respectively. Because of the similar peaked power profiles from both chlorine and copper, a unique fit for the relative contributions of these elements to the two sets of measured data cannot be made. Simultaneous soft X-ray measurements of radiated power profiles at a number of beryllium filter thicknesses would increase the reliability of the estimates of the relative proportions of each impurity element. Further experimental inputs, such as calibrated impurity line intensities from spectrometers or soft X-ray pulse height analysis measurements, would also increase the reliability of the estimates of Z_{eff}.

These simulations show that during the discharge the impurity density profiles with a central peak continuously increase, as the time constant for attaining equilibrium is much longer than the duration of the discharge. The consequent increase of the central radiated power and the decrease in net power to the plasma together with the slow central density rise, leads to a reduction of the central temperature which reinforces the increase in radiated power. A comparison of the radiation profiles of a density plateau discharge at a line integrated density of 1.6×10^{20} m^{-3} and a ramped density limit discharge reaching the same line integrated density is shown in Fig. 5. At the time when the diamagnetic energy is falling in both discharges the radiation profiles are peaked, suggesting that in both cases core radiation is the ultimate limitation for reaching higher densities. A divertor is currently being installed for W7-AS and should significantly reduce the level of impurity particle influx and allow steady state discharges to be achieved. The identified impurities in particular can be strongly reduced by component baking or shielding to restrict particle flux onto exposed surfaces.

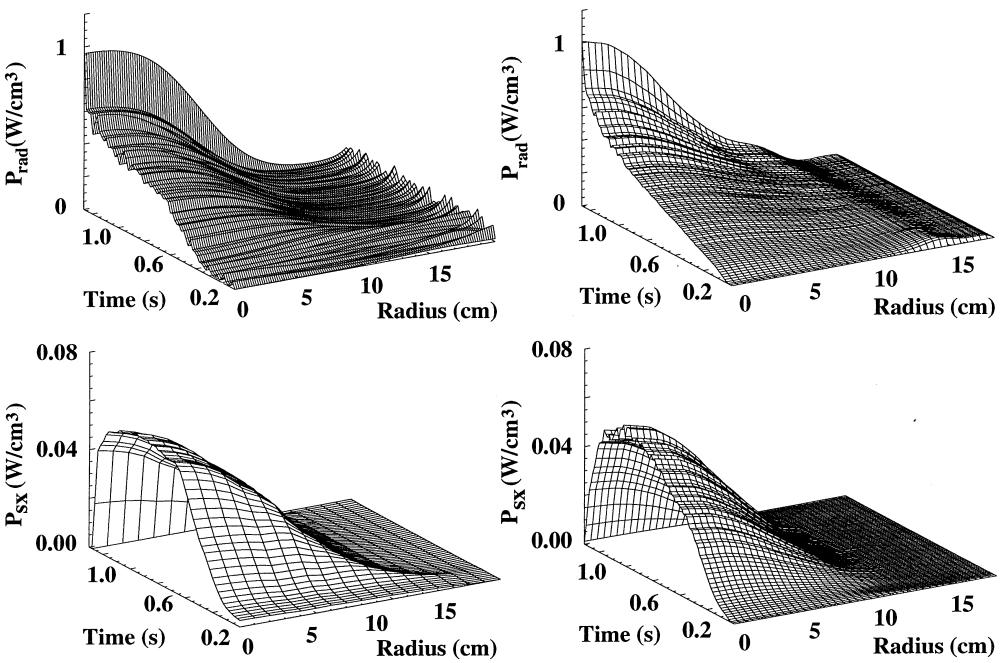

Fig. 4. A comparison of the measured (left column) and simulated (right column) radiation profiles for the density plateau discharge. The radiation profiles deduced from the bolometer and soft X-ray (12.5 μm Be filter) cameras are shown in the first and second rows, respectively. The bolometer and soft X-ray profiles were simulated using a diffusion coefficient and inward pinch coefficient profile calculated from Al laser blow-off experiments and time dependent electron temperature and density profiles with the impurity transport code STRAHL and the time dependent transport code ASTRA. Three impurity flux sources (C, Cl and Cu) at the plasma boundary were assumed.

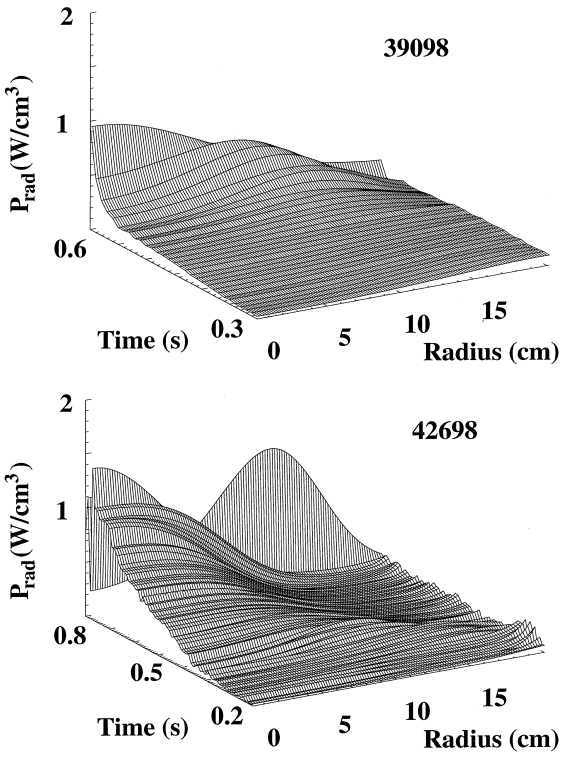

Fig. 5. A comparison of the radiation profiles of a density plateau discharge at a line integrated density of 1.6×10^{20} m^{-3} (bottom) and a ramped density limit discharge reaching the same line integrated density (top).

6. Conclusions

Modeling of density limit discharges with a modified two-point model can reproduce the features of a falling temperature and rising density in front of the limiter plates. The plasma detaches when the net power flux at the plasma edge decreases so that power balance in front of the limiter plate can no longer be fulfilled. The plasma collapsed rapidly after the total radiated power was greater than the NBI input power. The simple one-dimensional two-point model therefore describes the physics of the density limit in stellarators and tokamaks.

The time dependent simulation of the bolometer measurements and soft X-ray radiation measurements with a beryllium foil filter using density and temperature profiles, ASTRA, STRAHL and simple assumptions about the impurity flux at the boundary were carried out. This has proved to be a valuable tool for the interpretation of density limit discharges in W7-AS. The integration of further experimental measurements, such as calibrated impurity line intensities from spectrometers, soft X-ray pulse height analysis and simultaneous soft X-ray radiation power densities at a number of filter thicknesses, should be a goal for increasing the reliability of the estimates of Z_{eff}.

It was demonstrated that in the density plateau discharges the centrally peaked radial profile of the radiation power density was due to peaked impurity density profiles with a time constant for attaining equilibrium longer than the duration of the discharge. Decreasing net power to the plasma due to increasing radiated power from the plasma core is shown to be responsible for the observed fall in diamagnetic energy. The decrease of diamagnetic energy with time in density plateau discharges is influenced greatly by the vessel wall conditioning of helium glow discharges. Increased central temperatures and reduced total radiated power are then measured. The reduction of impurity fluxes to the discharge by the planned divertor for W7-AS will therefore be critical to achieving steady state operation at the highest possible density.

References

[1] U. Stroth et al., High confinement NBI discharges in the W7-AS Stellarator, submitted to Plasma Phys. Control. Fusion 40.
[2] G. Janeschitz et al., Plasma Phys. Control. Fusion 37 (1995) 11A, A19.
[3] G. Pereverzev et al., IPP Report 5/42, 1991.
[4] K. Borrass, Nucl. Fusion 31 (1991) 1035.
[5] K. Behringer, JET Report, JET-R(87)08, 1987.
[6] W-VIIA Team, NI Group, Nucl. Fusion 25 (1985) 1593.
[7] K. Borrass, Nucl. Fusion 33 (1993) 63.
[8] C.S. Pitcher, P.C. Stangeby, Plasma Phys. Control. Fusion 39 (1997) 779.
[9] P. Grigull et al., in: Proc. ITC-8 Conference, J. Plasma Fusion Research, to be published.
[10] W. Suttrop et al., Nucl. Fusion 37 (1997) 119.
[11] V. Mertens et al., in: Proc. 23rd EPS Conference on Contr. Fusion and Plasma Physics, vol. I, Kiev, 1996, p. 15.
[12] P.C. de Vries, J. Rapp, F.C. Schuller, M.Z. Tokar, Phys. Rev. Lett. 80 (1998) 3519.
[13] W. Suttrop et al., Plasma Phys. Control. Fusion 39 (1997) 2051.
[14] V. Mertens et al., Nucl. Fusion 37 (1997) 1607.
[15] R. Burhenn et al., in: Proc. 24th EPS Conference on Contr. Fusion and Plasma Physics, vol. IV, Berchtesgaden, 1997, p. 1659.